



Insight Into the Binding Mechanism of p53/pDIQ-MDMX/MDM2 With the Interaction Entropy Method

Mengxin Li^{††}, Yalong Cong^{††}, Yuchen Li¹, Susu Zhong¹, Ran Wang¹, Hao Li^{1,2} and Lili Duan^{1*}

¹ School of Physics and Electronics, Shandong Normal University, Jinan, China, ² Department of Science and Technology, Shandong Normal University, Jinan, China

OPEN ACCESS

Edited by:

Antonio Monari,
Université de Lorraine, France

Reviewed by:

Jean-Philip Piquemal,
Sorbonne Universités, France
José Pedro Cerón-Carrasco,
Universidad Católica San Antonio de
Murcia, Spain

*Correspondence:

Lili Duan
duanll@sdu.edu.cn

^{††}These authors have contributed
equally to this work

Specialty section:

This article was submitted to
Theoretical and Computational
Chemistry,
a section of the journal
Frontiers in Chemistry

Received: 03 October 2018

Accepted: 14 January 2019

Published: 29 January 2019

Citation:

Li M, Cong Y, Li Y, Zhong S, Wang R,
Li H and Duan L (2019) Insight Into the
Binding Mechanism of
p53/pDIQ-MDMX/MDM2 With the
Interaction Entropy Method.
Front. Chem. 7:33.
doi: 10.3389/fchem.2019.00033

The study of the p53-MDMX/MDM2 binding sites is a research hotspot for tumor drug design. The inhibition of p53-targeted MDMX/MDM2 has become an effective approach in anti-tumor drug development. In this paper, a theoretically rigorous and computationally accurate method, namely, the interaction entropy (IE) method, combined with the polarized protein-specific charge (PPC) force field, is used to explore the difference in the binding mechanism between p53-MDMX and p53-MDM2. The interaction of a 12mer peptide inhibitor (pDIQ), which is similar to p53 in structure, with MDMX/MDM2 is also studied. The results demonstrate that p53/pDIQ with MDM2 generates a stronger interaction than with MDMX. Compared to p53, pDIQ has larger binding free energies with MDMX and MDM2. According to the calculated binding free energies, the differences in the binding free energy among the four complexes that are obtained from the combination of PPC and IE are more consistent with the experimental values than with the results from the combination of the non-polarizable AMBER force field and IE. In addition, according to the decomposition of the binding free energy, the van der Waals (vdW) interactions are the main driving force for the binding of the four complexes. They are also the main source of the weaker binding affinity of p53/pDIQ-MDMX relative to p53/pDIQ-MDM2. Compared with p53-MDMX/MDM2, according to the analysis of the residue decomposition, the predicated total residue contributions are higher in pDIQ-MDMX/MDM2 than in p53-MDMX/MDM2, which explains why pDIQ has higher binding affinity than p53 with MDMX/MDM2. The current study provides theoretical guidance for understanding the binding mechanisms and designing a potent dual inhibitor that is targeted to MDMX/MDM2.

Keywords: polarized force field, interaction entropy, molecular dynamics simulations, binding free energy calculation, p53-MDMX/MDM2

INTRODUCTION

Protein-Protein interactions play an important role in the recognition of numerous biological processes and biomacromolecules (Pawson and Nash, 2000; Wang et al., 2001; Keskin et al., 2008). Investigating protein-protein interactions at the atomic level via MD simulation can yield quantitative information and is helpful for understanding the microscopic mechanisms of biological processes. Many vital biological processes, such as enzyme catalysis, gene expression,

and adjustment of signal pathways (Schreiber and Fersht, 1995, 1996; Pazos et al., 1997), are inseparable from the adjustment of protein interactions (Schreiber et al., 2009), which are at the heart of many essential biological processes. The design of drugs based on protein-protein interactions has become a hot topic. Since the origins of many diseases are closely related to protein disorders, the design of drugs that are aimed at regulating the structure, and function of proteins are becoming a focus of researchers. The binding strength between two proteins is determined by the binding free energy. Thus, accurate calculation of the binding free energy is vital for investigating the interaction mechanism and is helpful for drug design. Drug-like molecules tend to bind to hot areas (Burgoyne and Jackson, 2006; Cheung et al., 2012) in protein-protein interaction surfaces.

Molecular dynamics (MD) simulation (McCammon et al., 1977) is an important tool for exploring the characteristics of biomacromolecules. The accuracy of a simulation is determined by the force field that is used. However, the popular force fields, such as CHARMM, AMBER, GROMOS, and OPLS, do not consider the electrostatic polarization effect; hence, they may yield inaccurate results (Gao et al., 2011). In this study, the polarized protein-specific (PPC) force field, which fully considers the effect of electrostatic polarization, is used in the MD simulation. PPC is developed by the Zhang group (Ji et al., 2008) and many studies have demonstrated its advantage over the traditional force fields (Ji and Zhang, 2008; Duan et al., 2010, 2016a; Ji and Mei, 2014).

The calculation of the binding free energy between two proteins is the key issue in computer simulation and drug design. Precise free energy prediction methods can substantially improve the efficiency of drug design. At present, there are rigorous approaches to calculate the binding free energy, such as free energy perturbation (FEP) (Rao et al., 1987; Cummins and Gready, 1993) and thermodynamics integration (TI) (Straatsma and Berendsen, 1988; Aqvist et al., 1994). Although these methods are highly accurate (Chen et al., 2017a) in the calculation of the binding free energy, they are time-consuming and computationally expensive. In addition, they can only compute the relative binding free energy. In contrast, the Molecular Mechanics/Poisson-Boltzmann Surface Area (MM/PBSA) (Srinivasan et al., 1998; Wang and Kollman, 2000; Wang et al., 2001) method has been widely used in the calculation of absolute binding free energy due to its high efficiency (Sun et al., 2014; Genheden and Ryde, 2015; Chen et al., 2016). However, a serious problem with the MM/PBSA method is that calculating the entropic contribution is difficult. Typically, the normal mode (Nmode) method is used to compute the entropy change (Ngyuen and Case, 1985; Xu et al., 2011); this method is inaccurate for the study of biomacromolecules (Wang et al., 2016). In this paper, a novel method, namely, interaction entropy (IE) (Duan et al., 2016b), is used to calculate the entropy change, which is theoretically rigorous. It can yield more accurate results than the traditional Nmode method, which has been applied successfully to the calculation of the binding free energy in many studies (Duan et al., 2016a, 2017a,b; Aldeghi et al., 2017; Ben-Shalom et al., 2017; Cebrián-Prats et al., 2017; Chen et al., 2017a,b; Gao et al., 2017; Khammari et al., 2017; Nguyen

Quoc et al., 2017; Sun et al., 2017; Wang et al., 2017; Yan et al., 2017; Yang et al., 2017; Zarei et al., 2017; Zou et al., 2017; Cong et al., 2018; Liu et al., 2018; Qiu et al., 2018; Song et al., 2018).

Typically, residue decomposition is performed to obtain hot-spot residues in the MM/GBSA method (Martins et al., 2013; Simões et al., 2017). However, the entropy contribution cannot be computed via the Nmode method in the analysis of the residue decomposition, which results in overestimation of the predicted binding free energy of each residue. Fortunately, the IE method can calculate the entropy change of per residue, which overcomes this shortcoming of the traditional MM/GBSA method.

p53 is important tumor suppressor and transcription factor. It helps protect the integrity of the genome. The structures of oncoproteins MDMX and MDM2 are highly similar, which can inhibit the activation of p53. Overexpression of MDMX and MDM2 can cause function loss of p53, thereby resulting in the occurrence of cancer. According to numerous studies, more than 50% of malignant tumors are related to p53 (Vogelstein et al., 2000; Joerger and Fersht, 2007; Vazquez et al., 2008); hence, p53-MDMX/MDM2 interaction is an important target for tumor drugs. In many studies, drug design that is aimed at adjusting the p53 pathway is becoming popular. Chang et al. demonstrated that stapled α -helical peptide can be developed as an inhibitor of the interaction of p53 with MDMX and MDM2 (Chang et al., 2013). Tsuganezawa et al. developed a new method, namely, high-throughput screening (HTS) assay, for identifying drug inhibitors for the p53-MDMX interaction (Tsuganezawa et al., 2013). Verma et al. investigated the binding mechanism of a potential inhibitor, namely, polyphenol, to MDM2 via molecular docking and molecular dynamics simulation and found that luteolin has high inhibition potency for MDM2 (Verma et al., 2016). Few researchers have directly explored the interaction mechanisms between p53-MDMX and p53-MDM2, especially via the combination of PPC and IE methods. In addition, a peptide inhibitor, namely, pDIQ, that has high binding affinity for both MDMX and MDM2 was designed by Phan et al. (2010). For disrupting the interaction of p53-MDMX/MDM2 to maintain the activation of p53. In this paper, the binding mechanisms of p53-MDMX/MDM2 and pDIQ-MDMX/MDM2 are investigated via the combination of PPC and IE to obtain detailed binding information. The current work will provide important information for the design of dual-function inhibitors.

METHODS

MD Simulation

In current study, the initial structure of p53-MDMX (3DAB), p53-MDM2 (1YCR), pDIQ-MDMX (3JZQ), and pDIQ-MDM2 (3JZS) are obtained from Protein Databank (PDB). The parameters of the proteins are generated from the AMBER12SB force field. The Leap module is used to add all missing hydrogen atoms automatically. The four systems are solvated in the truncated periodic octahedral box of TIP3P waters to provide solvent environment, in which, the distance between the surface of the complex and the edge of the periodic box wall is 10 Å. The counter ions are added to neutralize the systems. To remove the steric clashes, the systems are relaxed by energy minimization,

which is performed by the steepest descent method, followed by conjugate gradient minimization. Then the whole systems are heated from 0 to 300 K up for 300 ps with the step of 2 fs. SHAKE (Ryckaert et al., 1977) algorithm is used to constrain all bonds involving hydrogen atoms. To prevent the unnecessary structural drift in protein-protein systems, the restrained MD simulations are performed up to 12 ns and 10 fs per frame is written to get enough conformational sampling from the last equilibrium stage for the four systems.

Molecular Mechanics/Poisson-Boltzmann Surface Area

In this paper, the MM/PBSA model (Massova and Kollman, 2000) is adopted to calculate the binding free energy. The binding free energy can be expressed by the following terms:

$$\Delta G_{bind} = G_{complex} - (G_{protein1} + G_{protein2}) \quad (1)$$

Where $G_{complex}$, $G_{protein1}$, $G_{protein2}$ represent the free energy of complex, p53/pDIQ, MDM2/MDMX, respectively. Additionally, the binding free energy is expressed by the sum of the following two terms:

$$\Delta G_{bind} = \Delta G_{gas} + \Delta G_{sol} \quad (2)$$

Where ΔG_{gas} , ΔG_{sol} represent the gas phase binding free energy and solvation free energy, respectively. ΔG_{gas} is divided into three terms:

$$\Delta G_{gas} = \Delta E_{ele} + \Delta E_{vdW} - T\Delta S \quad (3)$$

ΔE_{ele} , ΔE_{vdW} , and $-T\Delta S$ represent electrostatic interaction, van der Waals (vdW) interaction and entropic contribution, respectively.

The G_{sol} terms can be expressed by the sum of the polar and non-polar solvation free energy. The formula is as follows:

$$\Delta G_{solv} = \Delta G_{pb} + \Delta G_{np} \quad (4)$$

The first term of the formula is calculated by applying the PB equation. During the calculation, the internal, and external dielectric constants are set to 1 and 80, respectively. The second term ΔG_{np} can be calculated by the following formula:

$$\Delta G_{np} = \gamma \cdot SASA + \beta \quad (5)$$

SASA represents the solvent accessible surface area, which can be calculated by using the MSMS (Sanner et al., 1996) program. The values of γ and β are $0.00542 \text{ kcal} (\text{mol} \text{ \AA}^2)^{-1}$ and 0.92 kcal/mol , respectively. In our calculation, MM/PBSA method is performed based on 100 snapshots from MD simulation trajectory.

Interaction Entropy Method

In this paper, a new developed Interaction Entropy (IE) (Duan et al., 2016b, 2017a) method is applied to calculate the entropy change. All snapshots extracted from the last equilibrium MD simulation are used to the calculation of entropic contribution. This can be obtained from the following formula. The gas-phase component of the binding free energy for the interaction

of protein and protein can be expressed by the following equations:

$$\begin{aligned} \Delta G_{gas} &= -KT \ln \left[\frac{Q_{p1p2}}{Q'_{p1p2}} \right] \\ &= -KT \ln \frac{\int dq_w(p1p2) dq_{p1} dq_{p2} e^{-\beta(E_{p1}+E_{p2}+E_{p1-p2}^{int}+E_{w(p1p2)}+E_{p1p2-w}^{int})}}{\int dq_w(p1p2) dq_{p1} dq_{p2} e^{-\beta(E_{p1}+E_{p2}+E_{w(p1p2)}+E_{p1p2-w}^{int})}} \\ &= -KT \ln \left[\frac{1}{\langle e^{\beta E_{p1-p2}^{int}} \rangle} \right] \\ &= KT \ln \langle e^{\beta E_{p1-p2}^{int}} \rangle \\ &= \langle E_{p1-p2}^{int} \rangle + KT \ln \langle e^{\beta \Delta E_{p1-p2}^{int}} \rangle \\ &= \langle E_{p1-p2}^{int} \rangle - T\Delta S \end{aligned} \quad (6)$$

So the interaction entropy can be defined as the following equation:

$$-T\Delta S = KT \ln \langle e^{\beta \Delta E^{int}} \rangle \quad (7)$$

The ΔE^{int} is defined as the fluctuation of protein-protein interaction energy around the average energy. It can be expressed as the following equation:

$$\Delta E^{int} = E^{int} - \langle E^{int} \rangle \quad (8)$$

The $\langle E^{int} \rangle$ is averaged protein-protein interaction energy. This term of equation can be calculated by the formula:

$$\langle E^{int} \rangle = \frac{1}{N} \sum_{i=1}^N E^{int}(t_i) \quad (9)$$

The $\langle e^{\beta \Delta E^{int}} \rangle$ term of equation can be calculated by the formula:

$$\langle e^{\beta \Delta E^{int}} \rangle = \frac{1}{N} \sum_{i=1}^N e^{\beta \Delta E^{int}(t_i)} \quad (10)$$

For the above formulas, β represents $\frac{1}{KT}$.

RESULTS AND DISCUSSION

The Analysis of Stability

Prior to analyzing the binding free energy, to ensure the stability of the protein in the dynamic simulation and the convergence of the calculated interaction entropy, the root-mean-square deviation (RMSD) of the backbone atoms relative to the native structure is shown in **Figure S1** in Supporting Information. As shown in **Figure S1**, those structures of p53/pDIQ-MDMX/MDM2 are highly stable during MD simulation. **Figures 1A,B** show the interaction entropy as function of time in the 3DAB and 1YCR systems, respectively, where the black line represents the calculated results from

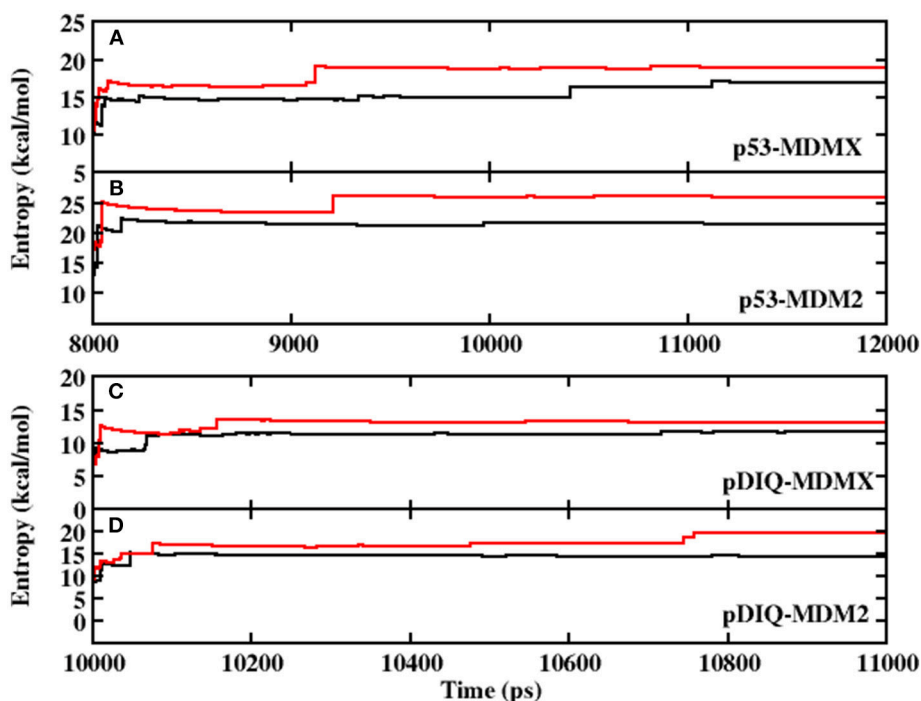


FIGURE 1 | The calculated interaction entropy under AMBER and PPC as a function of equilibrium time from MD simulation. **(A)** p53-MDMX system; **(B)** p53-MDM2 system; **(C)** pDIQ-MDMX; **(D)** pDIQ-MDM2.

AMBER and the red line represents the calculated results from PPC. The entropy change well converges in the MD simulation under the two force fields. In addition, the difference in the calculated entropy between AMBER and PPC is not large according to the figure; hence, the polarization effect has no substantial impact on the entropy change.

The Analysis of Binding Free Energy

To obtain detailed information on the binding mechanisms of p53-MDMX and p53-MDM2, the binding free energies are calculated under two combinations (AMBER-IE, PPC-IE). The results are listed in **Table 1**, in which the experimental values of 3DAB and 1YCR are -9.12 and -9.20 kcal/mol, respectively. The difference between the two experimental values is -0.08 kcal/mol. Under PPC-IE, the calculated binding free energies of 3DAB and 1YCR are -27.44 and -28.93 kcal/mol, respectively. The difference between them is -1.49 kcal/mol, which accords with the difference between the experimental values. However, the calculated binding free energies of 3DAB and 1YCR under AMBER-IE are -29.12 and -26.95 kcal/mol, respectively. The difference between the calculated binding free energies is 2.17 kcal/mol, which differs substantially from the experimental result. Additionally, the calculated standard deviations (STDs) in **Table 1** are all very low; hence, the results are reliable. The rank of the computed binding free energy is consistent with the rank of the experimental data under the PPC-IE method; therefore, PPC-IE is the superior choice and the following analysis will be based on the computations with PPC-IE. According to **Table 1**, the binding free energy of MDM2 with p53 is higher

than that of MDMX with p53. To further explore the binding mechanisms of p53 and MDM2/MDMX, the contributions of the binding free energy components are listed in **Table 2**. The binding energy of p53-MDMX is larger than that of p53-MDM2. Moreover, the electrostatic interactions, vdW interactions, and non-polar solvation energies contribute favorably to the binding free energy, while the polar solvation energy and entropy change play unfavorable roles.

In addition, although the electrostatic interaction plays a highly beneficial role, most of its favorable factors are offset by the unfavorable polar solvation energy. Therefore, the favorable binding energies of p53-MDMX/MDM2 are mainly provided by vdW interactions. Furthermore, we analyze the differences in the electrostatic term, vdW term, polar solvation energy, non-polar solvation energy, and entropy change between p53-MDMX and p53-MDM2, which are -19.35 , -180.38 , 192.87 , -1.63 , and 7.01 kcal/mol, respectively. The stronger binding energy of p53-MDM2 compared with p53-MDMX is mainly due to the vdW interactions.

The Analysis of Hydrogen Bond

To investigate the origin of the stronger binding affinity of p53 with MDM2 than with MDMX in detail, hydrogen bond analysis for p53-MDMX/MDM2 is performed and the hydrogen bond energy is calculated via the following formula (11) (Huang et al., 2008, 2012). The results are listed in **Table 3**.

$$\Delta G_{bind} = \frac{\alpha}{R^{12}} - \frac{\beta}{R^{10}} \quad (11)$$

TABLE 1 | Binding free energy for p53-MDMX/MDM2 and pDIQ-MDMX/MDM2 calculated by the combination of AMBER-IE and PPC-IE.

System	AMBER							PPC							ΔG_{exp}^*
	$\langle E_{\text{pp}}^{\text{int}} \rangle$	STD	-T ΔS	STD	ΔG_{sol}	STD	ΔG_{bind}	$\langle E_{\text{pp}}^{\text{int}} \rangle$	STD	-T ΔS	STD	ΔG_{sol}	STD	ΔG_{bind}	
P53-MDMX	-287.56	5.00	16.91	1.06	241.52	4.25	-29.12	-336.96	5.58	18.87	1.20	290.65	4.42	-27.44	-9.12
P53-MDM2	-480.66	6.04	21.45	0.68	432.26	5.04	-26.95	-536.69	6.90	25.88	1.35	481.89	5.44	-28.93	-9.20
$\Delta \Delta G$							2.17							-1.49	-0.08
PDIQ-MDMX	-201.31	4.18	11.82	0.68	163.05	3.27	-26.44	-237.69	4.65	13.14	0.73	196.33	3.72	-28.22	-9.5
PDIQ-MDM2	-372.41	4.81	14.47	0.69	320.47	3.49	-37.47	-402.49	5.39	19.66	1.60	351.71	4.30	-31.12	-11.0
$\Delta \Delta G$							-11.03							-2.90	-1.50

All values showed in the table in kcal/mol. *The experimental value is obtained from Holak et al. (Popowicz et al., 2007, 2008) and Chen et al. (Phan et al., 2010).

TABLE 2 | The energy terms under PPC-IE method for p53-MDMX/MDM2 and pDIQ-MDMX/MDM2 systems.

Component	p53-MDMX	p53-MDM2	Delta	PDIQ-MDMX	PDIQ-MDM2	Delta
ΔE_{vdW}	-60.30	-79.65	-19.35	-61.92	-69.50	-7.58
ΔE_{ele}	-276.66	-457.04	-180.38	-175.77	-332.99	-157.22
ΔG_{pol}	298.71	491.58	192.87	204.06	359.84	155.78
ΔG_{npol}	-8.06	-9.69	-1.63	-7.73	-8.13	-0.40
-T ΔS	18.87	25.88	7.01	13.14	19.66	6.52
$\Delta G_{\text{ele+pol}}$	22.05	24.85	2.80	28.29	26.85	-1.44
ΔG_{bind}	-27.44	-28.93	-1.49	-28.22	-31.12	-2.90

ΔE_{vdW} , ΔE_{ele} , ΔG_{pol} , ΔG_{npol} , -T ΔS , and $\Delta G_{\text{ele+pol}}$ represent van der Waals energy, electrostatic energy in the gas phase, polar solvation energy, non-polar solvation energy, entropy contribution, and the sum of the electrostatic energy with polar solvation energy, respectively. All values showed in the table are in kcal/mol.

TABLE 3 | Distance, occupancy, and energy of the hydrogen bonds formed from p53-MDMX/MDM2.

System	Donor	Acceptor	Distance (Å)	Occupancy (%)	Energy (kcal/mol)
p53-MDMX	LYS93-NZ-H	GLU110-OE1	2.75	99.94	-1.57
	TRP116-NE1-H	MET53-O	2.70	100.00	-2.87
	PHE112-N-H	GLN71-OE1	2.86	100.00	-1.31
p53-MDM2	TYR100-OH-HH	ASN122-O	2.58	100.00	-4.95
	TRP116-NE1-HE1	LEU54-O	2.78	100.00	-1.92
	PHE112-N-H	GLN72-OE1	2.96	100.00	-0.70
	ASN122-ND2-HD21	GLU25-OE1	2.90	100.00	-1.24

In the equation, α and β have values 5.571 and 668.580, respectively, and R is the distance of the H-acceptor for the hydrogen bond. To obtain detailed information on the hydrogen bond, we plot the distance between the hydrogen atom and acceptor vs. their frequency distributions in **Figure 2**. There are three hydrogen bonds in the p53-MDMX system, while four hydrogen bonds are found in p53-MDM2. For the system of p53-MDMX, the peaks of the distance distributions for TRP116HE1-MET53O, PHE112H-GLN71OE1, and LYS93HZ2-GLU110OE1 are at ~ 1.7 , 1.9, and 1.8 Å, respectively; hence, the formed hydrogen bonds are stable. For p53-MDM2, the peaks for TYR100HH-ASN122O, TRP116HE1-LEU54O, PHE112H-GLN72OE1, and ASN122HD21-GLU25OE1 are observed at 1.6, 1.8, 1.9, and 2.1 Å, respectively; hence, the formed hydrogen bonds are also highly stable. In addition, the time evolution of the hydrogen bond angle is shown in **Figure 3**. The angle remains

>120 throughout the simulation time; therefore, the hydrogen bonds are well preserved under the PPC force field.

According to the above analysis, MDM2 can form more hydrogen bonds than MDMX with p53. Additionally, the total energy of the hydrogen bonds in p53-MDM2 is higher than in p53-MDMX, according to **Table 3**. This may explain the stronger binding affinity in p53-MDM2 than in p53-MDMX.

The Decomposition of Residue

To explore the reason for the decline in the effectiveness of p53 against MDM2 in residues, residue decomposition is conducted and the p53-residue interaction spectrum is depicted in **Figure 4**. To obtain more detailed information about the hot-spot residues, the binding free energy is divided into vdW interactions, the sum of the electrostatic energy and the polar solvation energy,

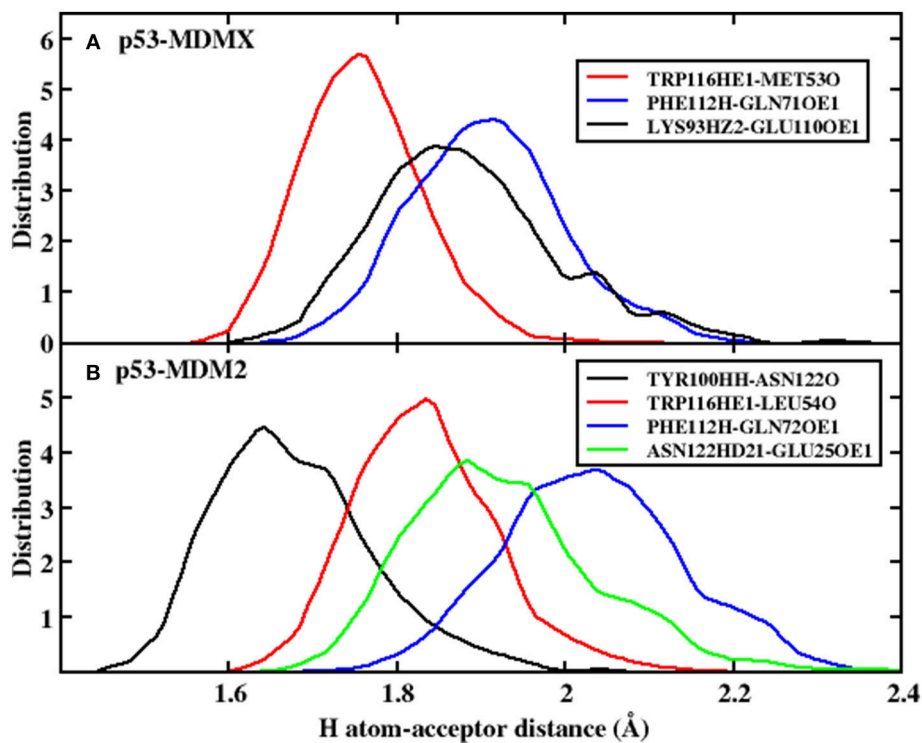


FIGURE 2 | The frequency distribution of the distance for H atom-acceptor. (A) p53-MDMX system; (B) p53-MDM2 system.

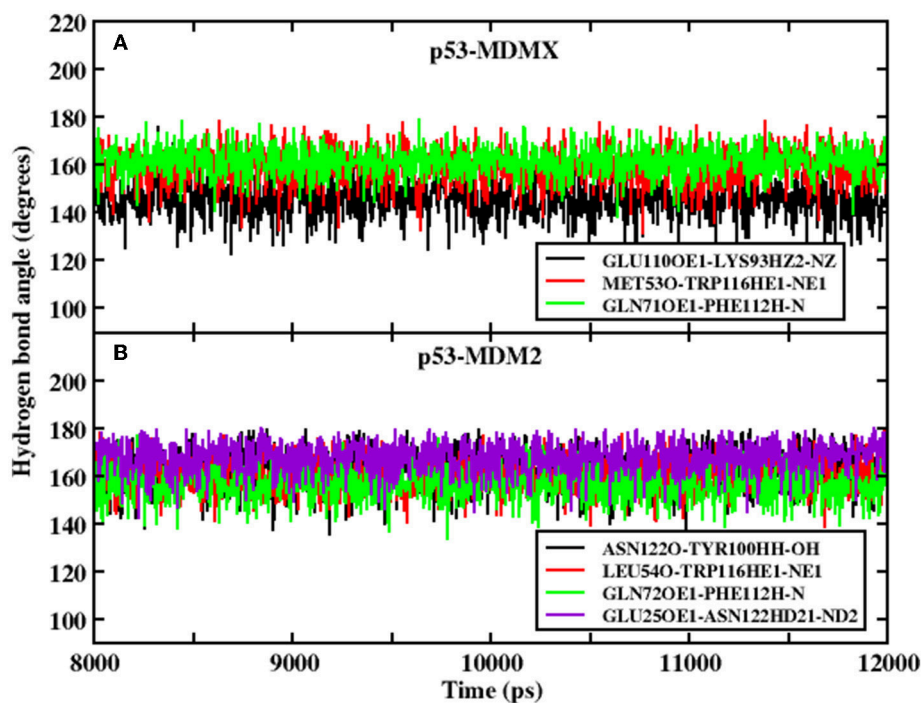


FIGURE 3 | Evolution of the hydrogen bond angle between p53 and MDMX/MDM2 under PPC force field. (A) p53-MDMX system; (B) p53-MDM2 system.

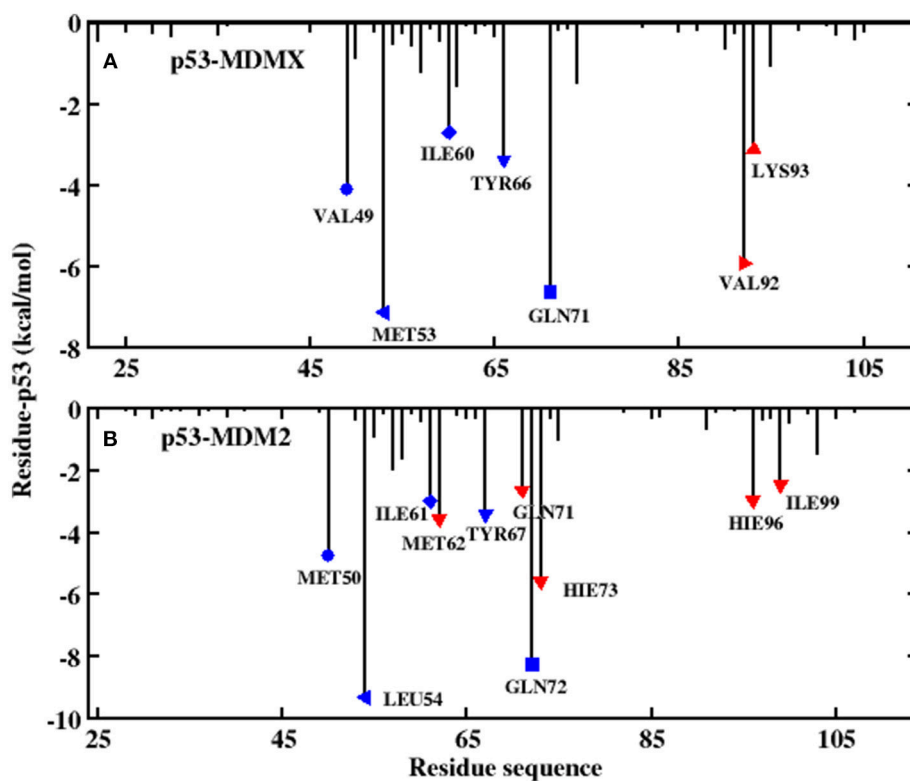


FIGURE 4 | Decomposition of the binding free energy toward per-residue. **(A)** p53-MDMX system; **(B)** p53-MDM2 system.

the non-polar solvation energy, and the entropy change for the systems, which are shown in **Figure 5**.

In this work, the decomposition of residues is performed via MM/GBSA, combined with the IE method. According to **Figure 4A**, there are a total of seven residues with an energy contribution of more than -2 kcal/mol in the p53-MDMX system, including VAL49, MET53, ILE60, TYR66, GLN71, VAL92, and LYS93. According to **Figure 5A**, the vdW interactions and non-polar solvation energy contribute favorably to binding, while the entropy change plays an unfavorable role in every residue. For the hot-spot residues of VAL49, ILE60, TYR66, GLN71, and VAL92, the vdW interactions provide a dominant favorable contribution to the binding free energy, while the energy contributions from residues MET53 and LYS93 are dominated by electrostatic energy. For the p53-MDM2 system, as shown in **Figure 4B**, there are a total of 10 residues with an energy contribution of more than -2 kcal/mol and they are MET50, LEU54, ILE61, MET62, TYR67, GLN71, GLN72, HIE73, HIE96, and ILE99. According to **Figure 5B**, MET50, ILE61, MET62, TYR67, GLN72, HIE73, HIE96, and ILE99 are primarily driven by the vdW interactions for binding with p53, while the sum of the electrostatic energy and the polar solvation energy play the substantial role in the binding of LEU54/GLN71-p53.

In order to get the specific explanation of the contribution for each hot-spot residue, the locations of the hot-spot

residues are shown in **Figure 6**. As shown in **Figure 6A**, in the p53-MDMX system, the alkyl of residue VAL49 and the alkyl of residue GLU121 can form a CH-CH hydrophobic interaction. For residue ILE60, the most important contribution to the binding energy comes from the CH- π hydrophobic term between the alkyl of residue ILE60 and the phenyls of residue PHE112. In addition, the alkyl of ILE60 with the indole of TRP116 also forms a CH- π hydrophobic interaction. The phenyl of residue TYR66 is near the phenyl of residue PHE112; hence, a π - π hydrophobic interaction is formed. The oxygen atom of GLN71 can form a CH-O interaction with the CH group of THR111. The hydrogen bond that is formed between PHE112 and GLN71 also plays an important role in the binding. The length, occupancy and energy of this hydrogen bond are 2.86 Å, 100%, and -1.31 kcal/mol, respectively, as listed in **Table 3**; therefore, the hydrogen bond is very stable. Residue VAL92 forms a CH-CH hydrophobic interaction between the alkyl of residue VAL92 and the alkyl of residue LEU115. According to the above analysis of the hydrogen bond that is described in **Table 3**, MET53 and TRP116 form a hydrogen bond interaction with a hydrogen bond length, occupancy and energy of 2.70 Å, 100%, and -2.87 kcal/mol, respectively. Residue LYS93 forms a hydrogen bond with GLU110, of which the length is 2.75 Å, the occupancy is 99.94%, and the energy is -1.57 kcal/mol. In addition, a hydrophobic interaction is formed between the alkyl of residue

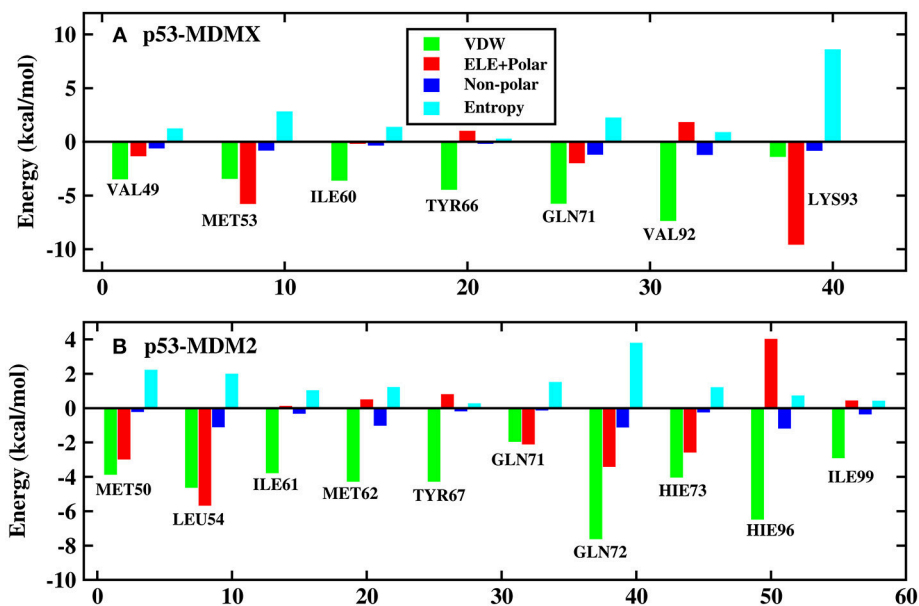


FIGURE 5 | Decomposition of the binding free energy on a per-residue basis into contributions from electrostatic interactions, vdW energy, polar solvation energy, and non-polar solvation energy. **(A)** p53-MDMX system; **(B)** p53-MDM2 system.

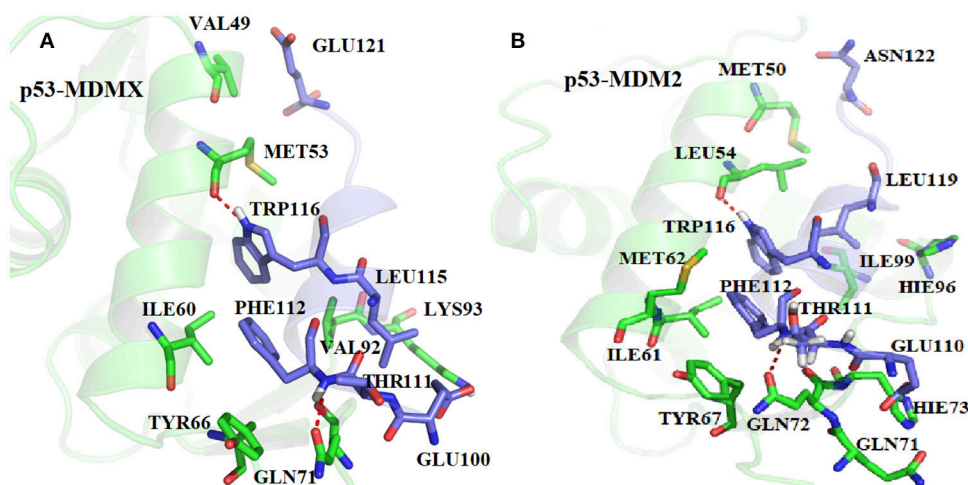


FIGURE 6 | The relative position of the key residues. **(A)** p53-MDMX system; **(B)** p53-MDM2 system.

LYS93 and the alkyl of residue LEU115, which also makes contributions.

According to, **Figure 6B**, the alkyl of MET50 and the alkyl of ASN122 form a CH-CH interaction. The CH group of ILE61 can interact with the indole of TRP116 and the benzene ring of PHE122. Residues MET62 and TYR67 are near residue PHE112; hence, it easy to produce a π -S interaction between MET62 and PHE112 and a π - π interaction between TYR67 and PHE112. The CH group of residue THR111 and the oxygen atom of GLN72 can form a CH-O interaction. Additionally, the oxygen atom of GLN72 forms a N-H group of residue PHE112, of

which the distance, occupancy and energy are 2.96 Å, 100%, and -0.7 kcal/mol, respectively, as listed in **Table 3**. The binding free energy between HIE73 and p53 mainly comes from the CH-O interaction. The binding energy of HIE96 with p53 mainly comes from the CH- π interaction between the imidazole of HIE96 and the alkyl of LEU119. The binding contribution of ILE99 mainly comes from the CH-CH interaction between alkyls of ILE99 and LEU119. LEU54 has the strongest binding free energy with p53 of all residues and the main energy contribution comes from two parts, namely, the hydrogen bond interaction, which has an energy of -1.92 kcal/mol, and the CH-CH vdW

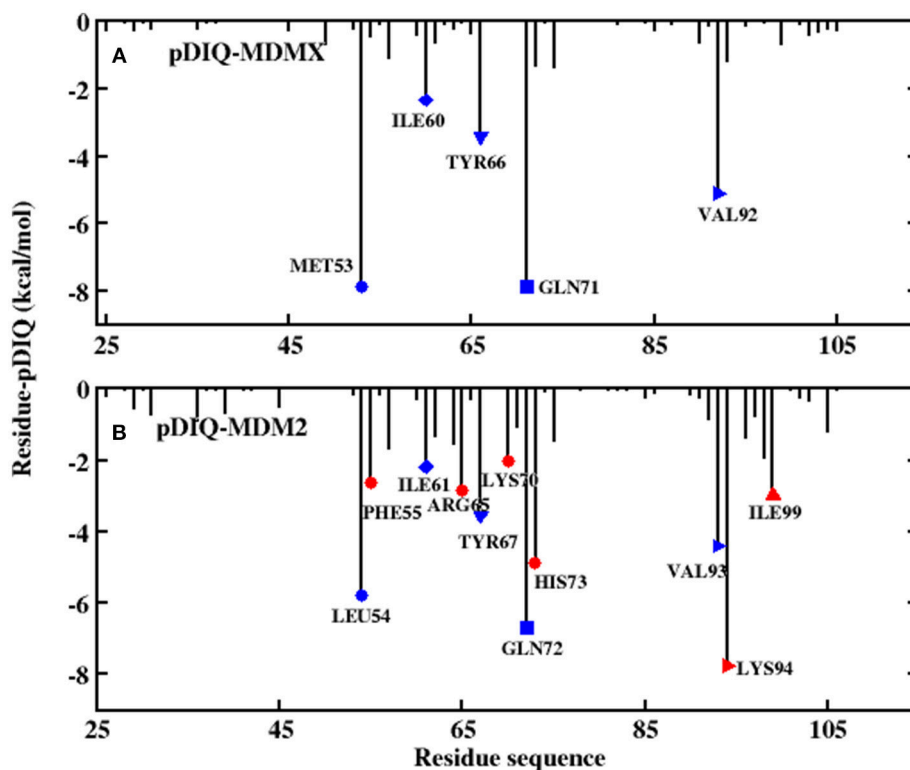


FIGURE 7 | Decomposition of the binding free energy toward per-residue. (A) pDIQ-MDMX system; (B) pDIQ-MDM2 system.

interaction that is formed between LEU54 and LEU119, as shown in **Figure 6B**. The CH-O interaction from residues GLN71 and GLU110 contributes substantially to the binding free energy. Based on the above analyses, the CH-CH, CH- π , CH-O, and π - π interactions are the main forces that drive the binding between MDMX/MDM2 and p53.

The Interaction Mechanism of pDIQ-MDMX/MDM2

Inhibiting efficiently the interaction of p53-MDMX/MDM2 can preserve the activation of p53, thereby preventing the occurrence of cancer. Therefore, in this paper, the interactions between an inhibitor, namely, pDIQ, and MDMX/MDM2 are also investigated to explore the binding mechanism.

The RMSD values of the backbone atoms relative to the native structure are plotted in **Figure S1** in the Supporting Information and the time evolution of the interaction entropy is plotted in **Figure 1**. According to these figures, the simulation well converged; hence, the following analysis are reliable. The calculated binding free energy of pDIQ-MDMX/MDM2 using PPC-IE is listed in **Table 1**. The difference in the binding free energy between pDIQ-MDMX and pDIQ-MDM2 of -2.90 kcal/mol is consistent with the difference between the experimental values of -1.50 kcal/mol. Additionally, according to the PPC-IE results, pDIQ has a stronger binding affinity with MDMX/MDM2 than p53. The calculated binding free energies for pDIQ-MDMX/MDM2 are -28.22

and -31.12 kcal/mol, respectively, while they are -27.44 and -28.93 kcal/mol in p53-MDMX/MDM2. pDIQ also has a stronger binding affinity with MDM2 than with MDMX. These results well agree with the experimental results.

Information on each energy component, including the electrostatic interactions, vdW interactions, non-polar solvation energies, polar solvation energy, and entropy change, for these two systems are listed in **Table 2**. Compared with pDIQ-MDMX, vdW interactions provide the major favorable contribution to the strong binding affinity in pDIQ-MDM2, which is consistent with the analysis of p53-MDMX/MDM2. To identify the contribution of every residue for the binding free energy to determine why pDIQ-MDM2 has higher binding ability than pDIQ-MDMX, the decomposition of residues is performed, the results of which are shown in **Figure 7**.

According to **Figure 5**, there are five common-location key residues for MDMX and MDM2: MET53, ILE60, TYR66, GLN71, and VAL92 in MDMX and LEU54, ILE61, TYR67, GLN72, and VAL93 in MDM2. In the pDIQ-MDM2 system, there are additional hot-spot residues that are not present in the pDIQ-MDMX system: PHE55, ARG65, LYS70, HIS73, LYS94, and ILE 99. The total energy contribution of the hot-spot residues in pDIQ-MDMX is less than in pDIQ-MDM2. This may be one of the reasons why pDIQ with MDMX has a weaker binding affinity than pDIQ with MDM2. Moreover, the contributions of the binding free energy for hot-spot residues

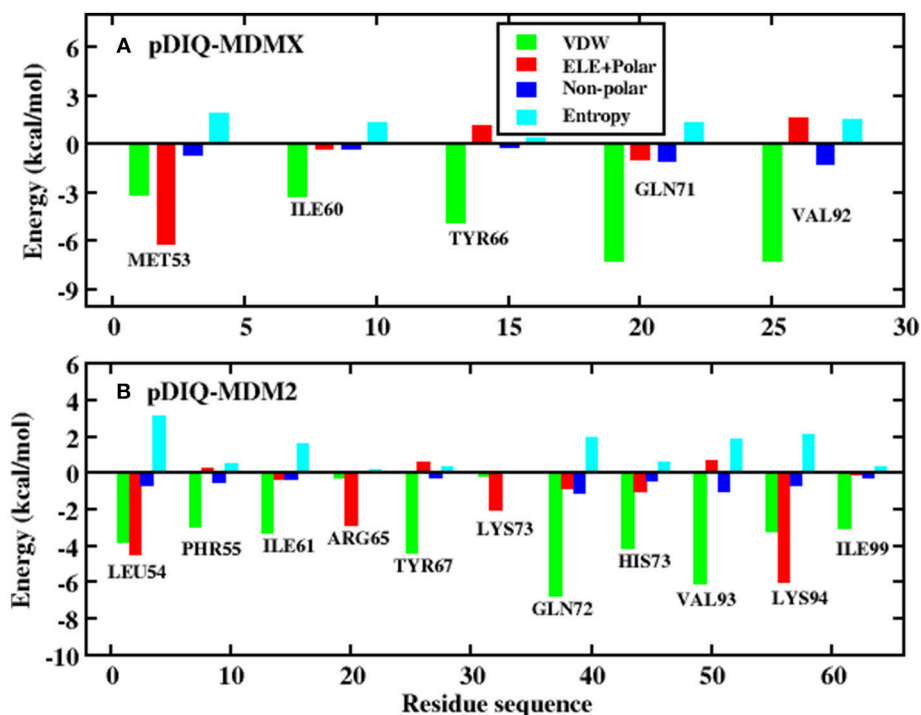


FIGURE 8 | Decomposition of the binding free energy on a per-residue basis into contributions from electrostatic interactions, vdW energy, polar solvation energy, and non-polar solvation energy. **(A)** pDIQ-MDMX system; **(B)** pDIQ-MDM2 system.

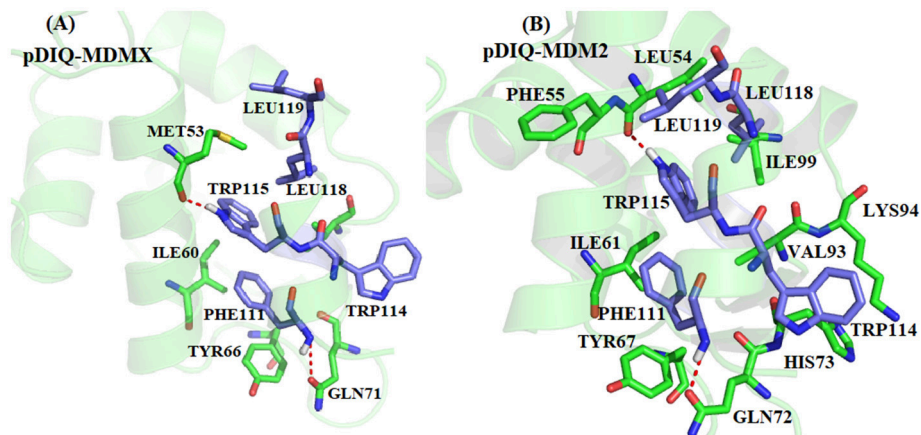


FIGURE 9 | The relative position of the key residues. **(A)** pDIQ-MDMX system; **(B)** pDIQ-MDM2 system.

are decomposed into detailed terms for the two complexes, as shown in **Figure 8**. For pDIQ-MDMX, the energies of residues ILE60, TYR66, GLN71, and VAL92 are dominated by the vdW interactions, while that of MET53 is dominated by the electrostatic interactions. Similarly, for MDM2-pDIQ, the main energy contributions of the hot-spot residues come from vdW interactions, except for LEU54, ARG65, and LYS94, for which the electrostatic interactions dominate the energy contributions.

The Analysis of p53 and pDIQ

According to both the calculation results and the experimental measurements, pDIQ exhibits a stronger binding affinity with MDM2/MDMX than p53. According to **Figures 4, 7**, the hot-spot residues in p53-MDMX are almost identical to those in pDIQ-MDMX; they are MET53, ILE60, TYR66, GLN71, and VAL92. The positions of key residues relative to pDIQ are depicted in **Figure 9**. According to **Figure 9A**, the locations of the key spots for pDIQ are almost same as in the description of p53-MDMX

in **Figure 6**. The binding modes of the key residues for p53-MDMX are similar to those for pDIQ-MDMX. However, the total residues contribution for pDIQ-MDMX is higher than for p53-MDMX, which results in a stronger binding affinity. For the p53-MDM2 and pDIQ-MDM2 systems, the main energy contribution comes from the six common residues: LEU54, ILE61, TYR67, GLN72, HIS73, and ILE99. They are also mainly dominated by the vdW interactions. Hot-spot residues that differ between the two systems are also identified: PHE55, ARG65, LYS70, VAL93, and LYS94 in pDIQ-MDM2 and MET50, MET62, GLN71, and HIE96 in p53-MDM2. The detailed interaction mechanism for each hot-spot residue with p53 has been explained in the previous analysis. Next, we analyze the hot-spot residues for pDIQ.

According to **Figure 9**, for PHE55-pDIQ, the energy contribution of -2.65 kcal/mol mainly comes from the CH- π interaction between the benzene ring of PHE55 and the alkyl of LEU119. The alkyl of VAL93 can generate interactions with the benzene ring of PHE111 and the indole of TRP 115, with a total energy contribution of -4.40 kcal/mol. For charged residue LYS 94, the binding free energy of -7.75 kcal/mol comes from the electrostatic interaction and the hydrophobic interaction between the alkyl of LYS93 and the indole of TRP114. For charged residues ARG65 and LYS70, the contributions to the binding energy are -2.86 and -2.02 kcal/mol, respectively, which mainly come from electrostatic interactions. The energy contributions of these hot-spot residues may lead to the difference in the binding affinity between p53-MDM2 and pDIQ-MDM2.

CONCLUSIONS

In this paper, the non-polarized AMBER force field and the PPC force field, combined with the newly developed IE method, are used to explore the interaction mechanisms of p53 and 12mer peptide inhibitor pDIQ with MDMX/MDM2. The PPC force field considers the surroundings of the amino acids and accurately expresses the polarization effect. In addition, the IE method makes full use of all samplings that are obtained from the MD simulation, thereby providing accurate and effective results without increasing the computational cost. The binding free energy is calculated via the combination of MM/PBSA and the IE method under the AMBER and PPC force fields, respectively. Our results demonstrate the following:

First, the difference in the calculated binding free energy between p53-MDMX/MDM2 and pDIQ-MDMX/MDM2 is

more consistent with the experimental difference that is observed under the PPC-IE method compared with AMBER-IE; hence, the electrostatic polarization effect plays an important role in the MD simulation. Moreover, the rank of the computed binding free energies are consistent with the rank of the experimental measurements under the PPC-IE method.

Second, according to the calculated binding free energy, the strength of MDM2 with p53 is stronger than that of MDMX with p53 because more hydrogen bonds are formed in p53-MDM2 than in p53-MDMX.

Third, according to the decomposition of the binding free energy, the vdW interactions are the main driving force for the binding in p53-MDMX/MDM2 and pDIQ-MDMX/MDM2. It is also the main cause of the weaker binding affinity of MDMX to p53/pDIQ compared with MDM2 to p53/pDIQ.

Fourth, pDIQ has stronger binding affinity with MDMX/MDM2 than p53 with MDMX/MDM2. The differences in the energy contributions of the hot-spot residues between the two systems lead to this phenomenon.

We hope this study can clarify the binding mechanisms of p53/pDIQ-MDMX/MDM2 and is helpful for designing a dual inhibitor that inhibits the p53-MDMX/MDM2 interaction.

AUTHOR CONTRIBUTIONS

ML and YC outperformed the MD simulations, drafted the main text of the manuscript, and prepared all the figures. YL, SZ, RW, and HL helped with data analysis. LD designed this study and revised the manuscript.

FUNDING

This work was supported by National Natural Science Foundation of China (Grant nos. 11774207, 11574184), the Natural Science Foundation of Shandong Province (ZR2016JL003), Primary Research & Development Plan of Shandong Province (No. 2017GSF18108).

SUPPLEMENTARY MATERIAL

The Supplementary Material for this article can be found online at: <https://www.frontiersin.org/articles/10.3389/fchem.2019.00033/full#supplementary-material>

REFERENCES

- Aldeghi, M., Bodkin, M. J., Knapp, S., and Biggin, P. C. (2017). Statistical analysis on the performance of molecular mechanics poisson-boltzmann surface area versus absolute binding free energy calculations: bromodomains as a case study. *J. Chem. Inf. Model.* 57, 2203–2221. doi: 10.1021/acs.jcim.7b00347
- Aqvist, J., Medina, C., and Samuelsson, J. E. (1994). A new method for predicting binding affinity in computer-aided drug design. *Protein Eng.* 7, 385–391. doi: 10.1093/protein/7.3.385
- Ben-Shalom, I. Y., Pfeiffer-Marek, S., Baringhaus, K.-H., and Gohlke, H. (2017). Efficient approximation of ligand rotational and translational entropy changes upon binding for use in MM-PBSA calculations. *J. Chem. Inf. Model.* 57, 170–189. doi: 10.1021/acs.jcim.6b00373
- Burgoyne, N. J., and Jackson, R. M. (2006). Predicting protein interaction sites: binding hot-spots in protein-protein and protein-ligand interfaces. *Bioinformatics* 22, 1335–1342. doi: 10.1093/bioinformatics/btl079
- Cebrián-Prats, A., Rovira, T., Saura, P., González-Lafont, À., and Lluch, J. M. (2017). Inhibition of mammalian 15-lipoxygenase by three ebselen-like drugs. A QM/MM and MM/PBSA comparative study. *J. Phys. Chem. A* 121, 9752–9763. doi: 10.1021/acs.jpca.7b10416
- Chang, Y. S., Graves, B., Guerlavais, V., Tovar, C., Packman, K., To, K. H., et al. (2013). Stapled α -helical peptide drug development: a potent dual inhibitor of

- MDM2 and MDMX for p53-dependent cancer therapy. *Proc. Natl. Acad. Sci. U.S.A.* 110, 3445–3454. doi: 10.1073/pnas.1303002110
- Chen, F., Liu, H., Sun, H., Pan, P., Li, Y., Li, D., et al. (2016). Assessing the performance of the MM/PBSA and MM/GBSA methods. 6. Capability to predict protein-protein binding free energies and re-rank binding poses generated by protein-protein docking. *Phys. Chem. Chem. Phys.* 18, 22129–22139. doi: 10.1039/C6CP03670H
- Chen, J., Wang, J., and Zhu, W. (2017a). Mutation L1196M-induced conformational changes and the drug resistant mechanism of anaplastic lymphoma kinase studied by free energy perturbation and umbrella sampling. *Phys. Chem. Chem. Phys.* 19, 30239–30248. doi: 10.1039/C7CP05418A
- Chen, J., Wang, J., and Zhu, W. (2017b). Zinc ion-induced conformational changes in new Delhi metallo- β -lactamase 1 probed by molecular dynamics simulations and umbrella sampling. *Phys. Chem. Chem. Phys.* 19, 3067–3075. doi: 10.1039/C6CP08105C
- Cheung, L. S. L., Kanwar, M., Ostermeier, M., and Konstantopoulos, K. (2012). A hot-spot motif characterizes the interface between a designed ankyrin-repeat protein and its target ligand. *Biophys. J.* 102, 407–416. doi: 10.1016/j.bpj.2012.01.004
- Cong, Y. L., Li, Y. C., Jin, K., Zhong, S. S., Zhang, J. Z. H., Li, H., et al. (2018). Exploring the reasons for decrease in binding affinity of HIV-2 against HIV-1 protease complex using interaction entropy under polarized force field. *Front. Chem.* 6:18. doi: 10.3389/fchem.2018.00380
- Cummins, P. L., and Gready, J. E. (1993). Computer-aided drug design: a free energy perturbation study on the binding of methyl-substituted pterins and N5-deazapterins to dihydrofolate reductase. *J. Comput. Aided Mol. Des.* 7, 535–555. doi: 10.1007/BF00124361
- Duan, L., Feng, G. Q., Wang, X., Wang, L., and Zhang, Q. (2017a). Effect of electrostatic polarization and bridging water on CDK2-ligand binding affinities calculated using a highly efficient interaction entropy method. *Phys. Chem. Chem. Phys.* 19, 10140–10152. doi: 10.1039/C7CP00841D
- Duan, L., Feng, G. Q., and Zhang, Q. G. (2016a). Large-scale molecular dynamics simulation: effect of polarization on thrombin-ligand binding energy. *Sci. Rep.* 6:31488. doi: 10.1038/srep31488
- Duan, L., Liu, X., and Zhang, J. Z. H. (2016b). Interaction entropy: a new paradigm for highly efficient and reliable computation of protein-ligand binding free energy. *J. Am. Chem. Soc.* 138, 5722–5728. doi: 10.1021/jacs.6b02682
- Duan, L., Zhu, T., Li, Y. C., Zhang, Q. G., and Zhang, J. Z. H. (2017b). Effect of polarization on HIV-1 protease and fluoro-substituted inhibitors binding energies by large scale molecular dynamics simulations. *Sci. Rep.* 7:42223. doi: 10.1038/srep42223
- Duan, L. L., Mei, Y., Zhang, D. W., Zhang, Q. G., and Zhang, J. Z. H. (2010). Folding of a helix at room temperature is critically aided by electrostatic polarization of intraprotein hydrogen bonds. *J. Am. Chem. Soc.* 132, 11159–11164. doi: 10.1021/ja102735g
- Gao, Y., Lu, X., Duan, L. L., Zhang, J. Z., and Mei, Y. (2011). Polarization of intraprotein hydrogen bond is critical to thermal stability of short helix. *J. Phys. Chem. B* 116, 549–554. doi: 10.1021/jp208953x
- Gao, Y., Zhang, C., Wang, X., and Zhu, T. (2017). A test of AMBER force fields in predicting the secondary structure of α -helical and β -hairpin peptides. *Chem. Phys. Lett.* 679, 112–118. doi: 10.1016/j.cplett.2017.04.074
- Genheden, S., and Ryde, U. (2015). The MM/PBSA and MM/GBSA methods to estimate ligand-binding affinities. *Expert Opin. Drug Discov.* 10, 449–461. doi: 10.1517/17460441.2015.1032936
- Huang, X., Zhao, X., Zheng, F., and Zhan, C. G. (2012). Cocaine esterase-cocaine binding process and the free energy profiles by molecular dynamics and potential of mean force simulations. *J. Phys. Chem. B* 116, 3361–3368. doi: 10.1021/jp2111605
- Huang, X., Zheng, F., Stokes, C., Papke, R. L., and Zhan, C. G. (2008). Modeling binding modes of $\alpha 7$ nicotinic acetylcholine receptor with ligands: the roles of Gln117 and other residues of the receptor in agonist binding. *J. Med. Chem.* 51, 6293–6302. doi: 10.1021/jm800607u
- Ji, C., and Mei, Y. (2014). Some practical approaches to treating electrostatic polarization of proteins. *Acc. Chem. Res.* 47, 2795–2803. doi: 10.1021/ar500094n
- Ji, C., Mei, Y., and Zhang, J. Z. (2008). Developing polarized protein-specific charges for protein dynamics: MD free energy calculation of pKa shifts for Asp26/Asp20 in thioredoxin. *Biophys. J.* 95, 1080–1088. doi: 10.1529/biophysj.108.131110
- Ji, C. G., and Zhang, J. Z. (2008). Protein polarization is critical to stabilizing AF-2 and helix-2' domains in ligand binding to PPAR- γ . *J. Am. Chem. Soc.* 130, 17129–17133. doi: 10.1021/ja807374x
- Joerger, A. C., and Fersht, A. R. (2007). Structural biology of the tumor suppressor p53. *Annu. Rev. Biochem.* 77, 557–582. doi: 10.1146/annurev.biochem.77.060806.091238
- Keskin, O., Gursoy, A., Ma, B., and Nussinov, R. (2008). Principles of protein-protein interactions: what are the preferred ways for proteins to interact? *Chem. Rev.* 39, 1225–1244. doi: 10.1021/cr040409x
- Khammari, A., Saboury, A. A., Karimijafari, M. H., Khoobi, M., Ghasemi, A., Yousefinejad, S., et al. (2017). Insights into the molecular interaction between two polyoxynated cinnamoylcoumarin derivatives and human serum albumin. *Phys. Chem. Chem. Phys.* 19, 10099–10115. doi: 10.1039/C7CP00681K
- Liu, X., Peng, L., Zhou, Y., Zhang, Y., and Zhang, J. Z. H. (2018). Computational alanine scanning with interaction entropy for protein-ligand binding free energies. *J. Chem. Theory Comput.* 14, 1772–1780. doi: 10.1021/acs.jctc.7b01295
- Martins, S. A., Perez, M. A., Moreira, I. S., Sousa, S. F., Ramos, M. J., and Fernandes, P. A. (2013). Computational alanine scanning mutagenesis: MM-PBSA vs TI. *J. Chem. Theory Comput.* 9, 1311–1319. doi: 10.1021/ct4000372
- Massova, I., and Kollman, P. A. (2000). Combined molecular mechanical and continuum solvent approach (MM-PBSA/GBSA) to predict ligand binding. *Perspect. Drug Discov. Des.* 18, 113–135. doi: 10.1023/A:1008763014207
- McCammon, J. A., Gelin, B. R., and Karplus, M. (1977). Dynamics of folded proteins. *Nature* 267, 585–590. doi: 10.1038/267585a0
- Nguyen Quoc, T., Hoang Linh, N., Huynh Quang, L., and Mai Suan, L. (2017). Protocol for fast screening of multi-target drug candidates: Application to Alzheimer's disease. *J. Mol. Graph. Model.* 77, 121–129. doi: 10.1016/j.jmgm.2017.08.002
- Nguyen, D. T., and Case, D. A. (1985). On finding stationary states on large-molecule potential energy surfaces. *J. Phys. Chem.* 89, 4020–4026. doi: 10.1021/j100265a018
- Pawson, T., and Nash, P. (2000). Protein-protein interactions define specificity in signal transduction. *Genes Dev.* 14, 1027–1047. doi: 10.1101/gad.14.9.1027
- Pazos, F., Helmer-Citterich, M., Ausiello, G., and Valencia, A. (1997). Correlated mutations contain information about protein-protein interaction. *J. Mol. Biol.* 271, 511–523. doi: 10.1006/jmbi.1997.1198
- Phan, J., Li, Z., Kasprzak, A., Li, B., Sebti, S., Guida, W., et al. (2010). Structure-based design of high affinity peptides inhibiting the interaction of p53 with MDM2 and MDMX. *J. Biol. Chem.* 285, 2174–2183. doi: 10.1074/jbc.M109.073056
- Popowicz, G. M., Czarna, A., and Holak, T. A. (2008). Structure of the human Mdmx protein bound to the p53 tumor suppressor transactivation domain. *Cell Cycle* 7, 2441–2443. doi: 10.4161/cc.6365
- Popowicz, G. M., Czarna, A., Rothweiler, U., Szwagierczak, A., Krajewski, M., Weber, L., et al. (2007). Molecular basis for the inhibition of p53 by Mdmx. *Cell Cycle* 6, 2386–2392. doi: 10.4161/cc.6.19.4740
- Qiu, L., Yan, Y., Sun, Z., Song, J., and Zhang, J. Z. H. (2018). Interaction entropy for computational alanine scanning in protein-protein binding. *Wiley Interdiscip. Rev. Comput. Mol. Sci.* 8:e1342. doi: 10.1002/wcms.1342
- Rao, S. N., Singh, U. C., Bash, P. A., and Kollman, P. A. (1987). Free energy perturbation calculations on binding and catalysis after mutating Asn 155 in subtilisin. *Nature* 328, 551–554. doi: 10.1038/328551a0
- Ryckaert, J. P., Ciccotti, G., and Berendsen, H. J. C. (1977). Numerical integration of the cartesian equations of motion of a system with constraints: molecular dynamics of n-alkanes. *J. Comput. Phys.* 23, 327–341. doi: 10.1016/0021-9991(77)90098-5
- Sanner, M. F., Olson, A. J., and Spehner, J. C. (1996). Reduced surface: an efficient way to compute molecular surfaces. *Biopolymers* 38, 305–320. doi: 10.1002/(SICI)1097-0282(199603)38:3<305::AID-BIP4>3.0.CO;2-Y
- Schreiber, G., and Fersht, A. R. (1995). Energetics of protein-protein interactions: analysis of the barnase-barstar interface by single mutations and double mutant cycles. *J. Mol. Biol.* 248, 478–486. doi: 10.1016/S0022-2836(95)80064-6
- Schreiber, G., and Fersht, A. R. (1996). Rapid, electrostatically assisted association of proteins. *Nat. Struct. Biol.* 3, 427–431. doi: 10.1038/nsb0596-427
- Schreiber, G., Haran, G., and Zhou, H. X. (2009). Fundamental aspects of protein-protein association kinetics. *Chem. Rev.* 109, 839–860. doi: 10.1021/cr800373w

- Simões, I. C. M., Costa, I. P. D., Coimbra, J. T. S., Ramos, M. J., and Fernandes, P. A. (2017). New parameters for higher accuracy in the computation of binding free energy differences upon alanine scanning mutagenesis on protein-protein interfaces. *J. Chem. Inf. Model.* 57, 60–72. doi: 10.1021/acs.jcim.6b00378
- Song, J., Qiu, L., and Zhang, J. Z. H. (2018). An efficient method for computing excess free energy of liquid. *Sci. China Chem.* 61, 135–140. doi: 10.1007/s11426-017-9106-3
- Srinivasan, J., Cheatham, T. E., Cieplak, P., Kollman, P. A., and Case, D. A. (1998). Continuum solvent studies of the stability of DNA, RNA, and phosphoramidate-DNA helices. *J. Am. Chem. Soc.* 120, 9401–9409. doi: 10.1021/ja981844+
- Straatsma, T. P., and Berendsen, H. J. C. (1988). Free energy of ionic hydration: analysis of a thermodynamic integration technique to evaluate free energy differences by molecular dynamics simulations. *J. Chem. Phys.* 89, 5876–5886. doi: 10.1063/1.455539
- Sun, H., Li, Y., Tian, S., Xu, L., and Hou, T. (2014). Assessing the performance of MM/PBSA and MM/GBSA methods. 4. Accuracies of MM/PBSA and MM/GBSA methodologies evaluated by various simulation protocols using PDBbind data set. *Phys. Chem. Chem. Phys.* 16, 16719–16729. doi: 10.1039/C4CP01388C
- Sun, Z. X., Yan, Y. N., Yang, M. Y., and Zhang, J. Z. H. (2017). Interaction entropy for protein-protein binding. *J. Chem. Phys.* 146:124124. doi: 10.1063/1.4978893
- Tsuganezawa, K., Nakagawa, Y., Kato, M., Taruya, S., Takahashi, F., Endoh, M., et al. (2013). A fluorescent-based high-throughput screening assay for small molecules that inhibit the interaction of MdmX with p53. *J. Biomol. Screening* 18, 191–198. doi: 10.1177/1087057112460729
- Vazquez, A., Bond, E. E., Levine, A. J., and Bond, G. L. (2008). The genetics of the p53 pathway, apoptosis and cancer therapy. *Nat. Rev. Drug Discov.* 7, 979–987. doi: 10.1038/nrd2656
- Verma, S., Grover, S., Tyagi, C., Goyal, S., Jamal, S., Singh, A., et al. (2016). Hydrophobic interactions are a key to MDM2 inhibition by polyphenols as revealed by molecular dynamics simulations and MM/PBSA free energy calculations. *PLoS ONE* 11:0149014. doi: 10.1371/journal.pone.0149014
- Vogelstein, B., Lane, D., and Levine, A. J. (2000). Surfing the p53 network. *Nature* 408, 307–310. doi: 10.1038/35042675
- Wang, C., Nguyen, P. H., Pham, K., Huynh, D., Le, T.-B. N., Wang, H., et al. (2016). Calculating protein-ligand binding affinities with MMPBSA: Method and error analysis. *J. Comput. Chem.* 37, 2436–2446. doi: 10.1002/jcc.24467
- Wang, J. M., Morin, P., Wang, W., and Kollman, P. A. (2001). Use of MM-PBSA in reproducing the binding free energies to HIV-1 RT of TIBO derivatives and predicting the binding mode to HIV-1 RT of efavirenz by docking and MM-PBSA. *J. Am. Chem. Soc.* 123, 5221–5230. doi: 10.1021/ja003834q
- Wang, W., and Kollman, P. A. (2000). Free energy calculations on dimer stability of the HIV protease using molecular dynamics and a continuum solvent model. *J. Mol. Biol.* 303, 567–582. doi: 10.1006/jmbi.2000.4057
- Wang, Y., Liu, J., Zhang, L., He, X., and Zhang, J. Z. H. (2017). Computational search for aflatoxin binding proteins. *Chem. Phys. Lett.* 685, 1–8. doi: 10.1016/j.cplett.2017.07.024
- Xu, B. S., Shen, H. J., Zhu, X., and Li, G. H. (2011). Fast and accurate computation schemes for evaluating vibrational entropy of proteins. *J. Comput. Chem.* 32, 3188–3193. doi: 10.1002/jcc.21900
- Yan, Y., Yang, M. Y., Ji, C. G., and Zhang, J. Z. H. (2017). Interaction entropy for computational alanine scanning. *J. Chem. Inf. Model.* 57, 1112–1122. doi: 10.1021/acs.jcim.6b00734
- Yang, Y. X., Li, S. Y., Zhang, Q., Chen, H., Xia, Z. N., and Yang, F. Q. (2017). Characterization of phenolic acids binding to thrombin using frontal affinity chromatography and molecular docking. *Anal. Methods* 9, 5174–5180. doi: 10.1039/C7AY01433C
- Zarei, O., Hamzeh-Mivehroud, M., Benvenuti, S., Ustun-Alkan, F., and Dastmalchi, S. (2017). Characterizing the hot spots involved in RON-MSPB complex formation using *in silico* alanine scanning mutagenesis and molecular dynamics simulation. *Adv. Pharm. Bull.* 7, 141–150. doi: 10.15171/apb.2017.018
- Zou, Y., Qian, Z., Sun, Y., Wei, G., and Zhang, Q. (2017). Orcein-related small molecule O4 destabilizes hIAPP protofibrils by interacting mostly with the amyloidogenic core region. *J. Phys. Chem. B* 121, 9203–9212. doi: 10.1021/acs.jpcc.7b08652

Conflict of Interest Statement: The authors declare that the research was conducted in the absence of any commercial or financial relationships that could be construed as a potential conflict of interest.

Copyright © 2019 Li, Cong, Li, Zhong, Wang, Li and Duan. This is an open-access article distributed under the terms of the Creative Commons Attribution License (CC BY). The use, distribution or reproduction in other forums is permitted, provided the original author(s) and the copyright owner(s) are credited and that the original publication in this journal is cited, in accordance with accepted academic practice. No use, distribution or reproduction is permitted which does not comply with these terms.